A language $\mathcal{L}$ is temporally invariant if it is mapped onto itself by the dynamic. Thus, we generate the image of $\mathcal{L}$ under the CA rule $\mathbf{\Phi}$:

$$\mathbf{\Phi}(\mathcal{L}) = \left\{ \mathrm{s}' : \mathrm{s}' = \Phi(\mathrm{s}),\ \mathrm{s} \in \mathcal{L} \right\} \tag{2}$$

The language is temporally invariant if $\mathbf{\Phi}(\mathcal{L}) = \mathcal{L}$. If $\mathcal{L}$ is a regular language, then so is $\mathbf{\Phi}(\mathcal{L})$, and the "finite machine evolution" (FME) algorithm developed in Ref. [8] gives a prescription for constructing $\mathbf{\Phi}(\mathcal{L})$ explicitly. This makes testing for invariance a practical task, even when $\mathcal{L}$ contains an infinite number of words, as is the case here. Application of the FME algorithm to the regular languages Λ^0 and Λ^1 shows that, under the action of CA rule 2614700074, they are both invariant: $\mathbf{\Phi}\left(\Lambda^0\right) = \Lambda^0$ and $\mathbf{\Phi}\left(\Lambda^1\right) = \Lambda^1$. This constitutes a computer proof of invariance. Details of this proof technique can be found, for a much simpler example, in Ref. [8].

The second defining characteristic of a regular domain, spatial homogeneity, is a form of spatial translation invariance. It is similar to statistical stationarity of the spatial pattern, and is defined in Ref. [8] as the requirement that the process graph of the domain be strongly connected. From Figure 2 it is obvious that the process graphs of Λ^0 and Λ^1 are strongly connected, and hence Λ^0 and Λ^1 are both spatially homogeneous. This completes the proof of the following result.

Proposition: Λ^0 and Λ^1 are regular domains.

3.2 Pattern Quantifiers

From the structure of the process graphs and the transition probabilities estimated from the reconstructed machines, we can directly calculate the spatial entropies and complexities of the domains.[13,14]

The topological entropy per symbol $h_0(\mathcal{L})$ of a regular language $\mathcal{L}$ is related to the exponential growth rate in number of distinct patterns in $\mathcal{L}$:

$$h_0(\mathcal{L}) = \lim_{L \to \infty} \frac{\log N_{\mathcal{L}}(L)}{L} \tag{3}$$

where $N_{\mathcal{L}}(L)$ is the number of distinct patterns (or "words") of length L in $\mathcal{L}$. From the minimal process graph $\mathrm{M}(\mathcal{L})$ of the domain language $\mathcal{L}$, we construct the connection matrix $\mathrm{T}(\mathcal{L})$ by setting each element t_{ij} of $\mathrm{T}(\mathcal{L})$ equal to the number of edges in $\mathrm{M}(\mathcal{L})$ that lead from state i to state j. Then $h_0(\mathcal{L})$ is given by the formula

$$h_0(\mathcal{L}) = \log \lambda_{\max} \tag{4}$$

where $\lambda_{\max}$ is the largest eigenvalue of $\mathrm{T}(\mathcal{L})$. Similarly, the metric entropy, which takes into account probabilistic structure of the domain, is defined as

$$h_1(\mathcal{L}) = \lim_{L \to \infty} -\frac{1}{L} \sum_{\substack{\omega \in \mathcal{L} \\ |\omega| = L}} p(\omega) \log p(\omega) \tag{5}$$

where $p(\omega)$ is the probability of occurrence of the word ω and the sum is taken over all distinct words of length L. The metric entropy is estimated from the empirical machine by

$$h_1(\mathcal{L}) = -\sum_{u \in \mathbf{V}} p(u) \sum_{\substack{v \in \mathbf{V} \\ \sigma \in \mathcal{A}}} p_{\substack{u \to v \\ \sigma}} \log p_{\substack{u \to v \\ \sigma}} \tag{6}$$

where $\mathbf{V}$ is the set of states of $\mathrm{M}(\mathcal{L})$, $p(u)$ is the asymptotic probability of visiting state u and $p_{u \to v}^{\sigma}$ is transition probability from state u to state v on symbol σ, i.e., the probability that the machine will move into state v upon receiving the symbol σ as input, given that it is currently in state u.

The (finitary) topological and statistical complexities of a regular language, $C_0(\mathcal{L})$ and $C_1(\mathcal{L})$ respectively, are related to the amount of "memory" in the process that generates that language, and are given as

$$\begin{aligned} C_0(\mathcal{L}) &= \log \|\mathbf{V}\| \\ C_1(\mathcal{L}) &= -\sum_{v \in \mathbf{V}} p(v) \log p(v) \end{aligned} \tag{7}$$

where again, $\mathbf{V}$ is the set of states in the minimal process graph of $\mathcal{L}$, $\|\mathbf{V}\|$ is the cardinality of $\mathbf{V}$, and $p(v)$ is the asymptotic probability of visiting state v. More information on $C_0(\mathcal{L})$ and $C_1(\mathcal{L})$, and on the calculation of entropy and complexity of a language from its minimal process graph, can be found in Refs. [13,14].

Table 1 shows the entropies and complexities of the domains Λ^0 and Λ^1, as calculated from their process graphs. The interesting thing to note is that the two domains differ in both entropy and complexity: Λ^0 has higher entropy, and lower complexity, than Λ^1. For each domain $h_0 = h_1$, indicating that the branching states in each domain have equal transition probabilities. Because the process graphs of both Λ^0 and Λ^1 are cyclic loops, and because the single branching state has equal branch probabilities, $C_0 = C_1$ as well. In general, however, the metric and topological quantities are related by $h_1 \leq h_0$, $C_1 \leq C_0$.[†]

The invariance of the domain languages, proved using the FME operator, implies the spatial and temporal invariance of the topological entropy and complexity densities h_0 and C_0 within each domain. The equivalent proof of invariance of the metric quantities h_1 and C_1 uses an extension of the FME operator to machines with probabilities on the edges. We chose a different tack here, however. For each domain Λ^i, we generated a random initial condition $\mathrm{s}_0 \in \Lambda^i$ of size $N = 1 \times 10^6$ and allowed it to evolve under the CA rule for $t = 200$ steps. We then applied machine reconstruction to both s_0 and s_{200}, and measured the metric entropy and statistical complexity at the two times. The comparison showed that for both Λ^0 and Λ^1, h_1 and C_1 are invariant.

The next pair of quantities we measure relate to the single-site statistics of states in the ensemble. Again, there are topological and metric versions of this. The metric quantity, $\rho_1(\mathcal{L})$, is the fraction of cells with nonzero values, averaged over all states in the ensemble:

$$\rho_1(\mathcal{L}) = \|\mathcal{L}\|^{-1} \sum_{\omega \in \mathcal{L}} \frac{1}{|\omega|} \sum_{i=1}^{|\omega|} \Theta(\sigma^i) \tag{8}$$

where $\|\mathcal{L}\|$ is the cardinality of $\mathcal{L}$, σ^i is the $i\mathrm{th}$ symbol of ω, and $\Theta(\sigma) = 0$ if $\sigma = 0$ and $\Theta(\sigma) = 1$ for all $\sigma \neq 0$.[‡] The corresponding topological quantity, $\rho_0(\mathcal{L})$, is the fraction of

[†]Because the equal branching probabilities, the fluctuation spectra (see [15]) for the domains are both single points.

[‡]This is the formula for $\mathcal{L}$ finite, which is used in numerical Monte Carlo estimates or estimates made at fixed lattice size N. For $\mathcal{L}$ infinite, we restrict eq. 8 to words of length $|\omega| = L$, and then take the limit $L \to \infty$.

nonzero cells in the CA lookup table outputs of parent neighborhoods occurring in $\mathcal{L}$. The set $\Pi_{\mathcal{L}}$ of parent neighborhoods in $\mathcal{L}$ is identical to the set of words in $\mathcal{L}$ of length $2r+1$, where r is the radius of the CA rule:

$$\Pi_{\mathcal{L}} = \{\omega : \ \omega \in \mathcal{L}, \ |\omega| = 2r+1\} \tag{9}$$

Then $\rho_0(\mathcal{L})$ is just the fraction of the set $\Pi_{\mathcal{L}}$ that map to nonzero values under the rule:

$$\rho_0(\mathcal{L}) = \frac{\sum\limits_{\substack{\sigma \in \mathcal{A} \\ \sigma \neq 0}} \eta_{\mathcal{L}}(\sigma)}{\sum\limits_{\sigma \in \mathcal{A}} \eta_{\mathcal{L}}(\sigma)} \tag{10}$$

where $\eta_{\mathcal{L}}(\sigma)$ is the number of parent neighborhoods in $\Pi_{\mathcal{L}}$ that map to the value σ under the CA rule ϕ. If all possible parent neighborhoods occur in the ensemble $\mathcal{L}$, then $\rho_0(\mathcal{L})$ is equivalent to the "lambda parameter" defined in [16]. Our choice of notation for these quantities emphasizes the ensemble-dependence of their definitions and differentiates them from the "Lyapunov exponents" defined below. The values of ρ_0 and ρ_1 for both domains are shown in Table 1. The large difference between the values of $\rho_1(\Lambda^0)$ and $\rho_1(\Lambda^1)$ is what makes the two domains so easy to identify visually in Figure 1. However, we must emphasize that $\rho_0(\mathcal{L})$ does not reflect the domains' evolution, and so may or may not be relevant, and $\rho_1(\mathcal{L})$ is not indicative of the domains' structural regularity.

The final row in Table 1 gives the values of the left- and right-Lyapunov exponents λ_L and λ_R, discussed in Section 3.4 below.

Quantifier	Λ^0	Λ^1	$\mathbf{\Phi}_t(\mathcal{A}^*)$
h_0	1/2	1/4	0.9(†)
h_1	0.500	0.250	0.7(†)
C_0	1	2	5.5(†)
C_1	1.000	2.000	2.1(†)
ρ_0	4/11	6/10	15/32
ρ_1	0.250	0.625	0.41(†)
λ_L, λ_R	-2, 2	-2, 2	-1.64, 1.73

Table 1 Quantifiers for the two domains Λ^0 and Λ^1, and for the full state space $\mathcal{A}^*$. See the text for definitions of the quantifiers. Fractional numbers and integers without decimal points are exact quantities. All others were estimated numerically, and have an uncertainty of ± 1 in the last decimal place. Numbers marked with the symbol (†) are nonstationary quantities, and were measured on a lattice of size $N = 1 \times 10^6$ at time $t = 200$.

For comparison, we have also included a third column in Table 1 that gives estimates of values of the domain quantifiers for the full state space $\mathcal{A}^*$. This is despite the fact that most of the quantifiers are nonstationary, due to the global contraction of the state space under the dynamic, i.e.,

$$\mathbf{\Phi}_{t+1}(\mathcal{A}^*) \subset \mathbf{\Phi}_t(\mathcal{A}^*), \ \forall t \geq 0 \tag{11}$$

and generally to the creation and annihilation of domains, walls, particles, and other structures. For example, the topological complexity $C_0(\mathbf{\Phi}_t(\mathcal{A}^*))$ appears to grow without bound, as the number of states in the machines for the sequence of languages $\{\mathbf{\Phi}_t(\mathcal{A}^*),\ t = 0, 1, 2, ...\}$ rapidly diverges under the action of the FME operator.[17] For the entropies, complexities, and single-site statistics in Table 1, we estimated the values using a single state s_t evolved from a random initial condition $\mathrm{s}_0 \in \mathcal{A}^*$ of size $N = 1 \times 10^6$, iterated up to time $t = 200$. The entropies $h_0(\mathbf{\Phi}_t(\mathcal{A}^*))$ and $h_1(\mathbf{\Phi}_t(\mathcal{A}^*))$, and the density of nonzero cells $\rho_1(\mathbf{\Phi}_t(\mathcal{A}^*))$ were estimated from the statistics of subsequences of s_t of length $L = 18$. The complexities $C_0(\mathbf{\Phi}_t(\mathcal{A}^*))$ and $C_1(\mathbf{\Phi}_t(\mathcal{A}^*))$ were estimated by the topological and metric total excess entropies, again measured over subsequences of length $L = 18$.[18] The (topological) fraction of nonzero cells $\rho_0(\mathbf{\Phi}_t(\mathcal{A}^*))$, being a property of the rule table and initial ensemble alone, was calculated exactly.

The most important thing to realize from the comparison between the values of domain quantities for the two domains on the one hand, and the full state space on the other, is that the global average can be misleading. The average density ρ_1, for example, is misleading in the same way that the mean of a bimodal distribution is misleading: it fails to capture the fact that there are two distinct types of behavior. For example, take any small region of space-time in the evolution of a random initial condition. Typically, this region is in one or the other domain. The density of nonzero cells in the region is not halfway between the densities of the two domains, it is simply one or the other. That is, there is no region in which the density of nonzero cells is $\rho_1 \approx 0.41$. Excepting the domain wall regions, which do not play a dominant role in the average (though for other rules they could), there are only regions with a density of nonzero cells close to either $\rho_1 \approx 0.25$ or $\rho_1 \approx 0.63$.

3.3 Domain Difference Patterns

One graphical measure of the structure of information flow in a CA is the *difference pattern*.[19] Here we introduce two important modifications of this technique. We refer to the resulting method as domain-dependent difference patterns. The consequences are striking and demonstrate the important structural role played by regular domains.

To generate a difference pattern, we start with a given "fiducial" state $\mathrm{s}_0 = ...\sigma_0^{i-1}\sigma_0^i\sigma_0^{i+1}...$ in some pattern ensemble $\mathcal{L}$ and create a new state $\widetilde{\mathrm{s}_0} = ...\tilde{\sigma}_0^{i-1}\tilde{\sigma}_0^i\tilde{\sigma}_0^{i+1}...$ that differs from s_0 in a single cell. This is done by adding to s_0 the perturbation δ^j consisting of a single nonzero cell at site j: $\sigma^j = 1$, $\sigma^{i\neq j} = 0$; this is the smallest possible variation in the local state. The result is

$$\widetilde{\mathrm{s}_0} = \mathrm{s}_0 \dot{+} \delta^j \tag{12}$$

where "$\dot{+}$" denotes cell-by-cell addition modulo $k = \|\mathcal{A}\|$, the alphabet size. In addition, we require that cell j be chosen so that the perturbed state $\widetilde{\mathrm{s}_0}$ is still in $\mathcal{L}$; for Λ^0 and Λ^1, this is accomplished by requiring that cell j be a wild-card. Both the fiducial and perturbed states are iterated independently using the CA rule, and at each time step we plot the difference pattern

$$\mathbf{\Delta}_t^{\mathcal{L}} = \mathrm{s}_t \dot{-} \widetilde{\mathrm{s}_t} \tag{13}$$

where $\dot{-}$ is subtraction modulo k. The resulting picture shows the space-time cells whose values are dependent on the value of the perturbed cell σ_0^j. Not surprisingly, the difference pattern is

dependent on the particular choice of initial condition s_0. Figure 5 shows space-time plots of the difference patterns $\mathbf{\Delta}_t^{\mathcal{L}}$ generated by states chosen randomly from three different sets: $\mathcal{L} = \mathcal{A}^N$ (Figure 5(a)), $\mathcal{L} = \Lambda^0$ (Figure 5(b)), and $\mathcal{L} = \Lambda^1$ (Figure 5(c)). In each case, the evolution was on a lattice of size $N = 100$ with periodic boundary conditions, and the perturbed cell was located at $j = N/2$. Note that for each of these patterns, the maximum instantaneous rate at which the perturbation spreads in either direction is equal to the "speed of light" of this rule, $c = 2$ cells/iteration. However, beneath this spreading light cone, the patterns differ markedly. The difference pattern $\mathbf{\Delta}_t^{\mathcal{A}^N}$ for $\mathrm{s}_0 \in \mathcal{A}^N$ shows an irregular structure, while the patterns for the domains Λ^0 and Λ^1 both have the same regular structure. The latter two are in fact identical to each other, $\mathbf{\Delta}_t^{\Lambda^0} = \mathbf{\Delta}_t^{\Lambda^1}$ for all t. When every other cell in space is removed — using the decimation operator $\mathrm{T}_{\mathrm{decimate}}(\Lambda)$ of Ref. [8] — they are identical to the space-time diagram of the chaotic, linear elementary CA rule 90 with an initial condition consisting of a single nonzero cell. That is,

$$\mathrm{T}_{\mathrm{decimate}}\left(\mathbf{\Delta}_t^{\Lambda^i}\right) = \Phi_t^{90}(0^*10^*) \tag{14}$$

3.4 Domain Difference Plumes

To investigate the statistical information transmission properties of an entire ensemble, we use the *difference plume*, or averaged difference pattern. For each state s_0 in an ensemble $\mathcal{L}$, we form the difference pattern as above, creating an ensemble of "difference pairs" for a given perturbation δ^j: $\left\{(\mathrm{s}_0, \widetilde{\mathrm{s}_0}) \,:\, \widetilde{\mathrm{s}_0} = \mathrm{s}_0 \dot{+} \delta^j,\ \mathrm{s}_0, \widetilde{\mathrm{s}_0} \in \mathcal{L}\right\}$. As above, both the original and the perturbed state must be in the ensemble; i.e. the $\sigma^j = 1$ in δ^j appears only at wild card sites. Then at each point (i,t) in space-time, we average $\Delta_t^i = \sigma_t^i \dot{-} \tilde{\sigma}_t^i$ over the ensemble:

$$\left\langle \Delta_t^i \right\rangle = \|\mathcal{L}\|^{-1} \sum_{\mathrm{s}_t \in \mathcal{L}} \Delta_t^i \tag{15}$$

Thus $\left\langle \Delta_t^i \right\rangle$ is the fraction of difference pairs for which $\sigma_t^i \neq \tilde{\sigma}_t^i$. At $t = 0$, for example, $\left\langle \Delta_0^i \right\rangle = 1$ for $i = j$ and $\left\langle \Delta_0^i \right\rangle = 0$ for all $i \neq j$.

The difference plumes for the three ensembles $\mathcal{A}^N$, Λ^0, and Λ^1 are shown in Figures 6(a), 6(b), and 6(c), respectively. Each plume was calculated using a Monte Carlo sample of 1000 state pairs on a lattice of size $N = 100$, with the perturbation in cell $j = N/2$. The difference plume for $\mathcal{A}^N$ (Figure 6(a)) is devoid of internal structure, with $\left\langle \Delta_t^i \right\rangle$ smoothly decreasing toward the edges of the light cone. The plumes for Λ^0 and Λ^1 are quite different from this. In both of the latter, the averaged difference plume is identical to the difference pattern generated by a single initial condition. At each space-time point (i,t), $\left\langle \Delta_t^i \right\rangle$ is either identically zero or one. Thus all states in Λ^0 have the same difference pattern—i.e., the propagation of information is identical for all states in the ensemble. The situation is exactly the same for Λ^1, even though the two domains have strikingly different spatial structure. The important thing to note is that, without having identified the ensembles Λ^0 and Λ^1, we would never have noticed any structure in the difference plumes at all. The average over all of state space washes it out entirely.

Three quantitative measures of the plume serve to emphasize this difference. First, we measure the average rate at which the difference plume spreads. This is given by the two quantities $\lambda_L(\mathcal{L})$, $\lambda_R(\mathcal{L})$, which are the linearized average velocities of the left and right edges

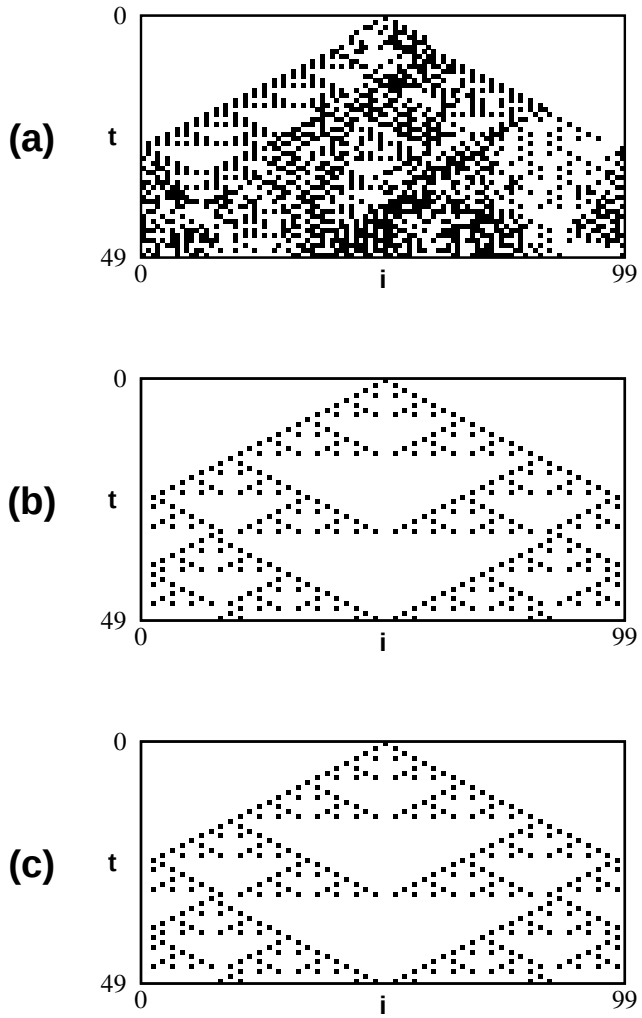

Figure 5 Difference patterns $\Delta_t^{\mathcal{L}}$: (a) $\mathcal{L} = \mathcal{A}^N$. Global difference pattern in which the initial condition was randomly selected over the entire state space: $s_0 \in \mathcal{A}^N$; (b) random IC in domain $\mathcal{L} = \Lambda^0$; (c) random IC in domain $\mathcal{L} = \Lambda^1$. In each plot, evolution was on a lattice of size $N = 100$ and the initial condition was perturbed in cell $j = 50$. The patterns of (b) and (c) are identical, and are also identical to an "expanded" space-time diagram of elementary CA rule 90 in which a 0 is inserted between every horizontal pair of cells.

of the plume, respectively. These are the left- and right-Lyapunov exponents [20,21] restricted to the ensemble $\mathcal{L}$. They are defined as follows.

For each difference pattern in the ensemble, denote the leftmost and rightmost cells σ_t^i for which $\Delta_t^i \neq 0$ by $\mathrm{Left}(\Delta_t)$ and $\mathrm{Right}(\Delta_t)$. That is,

$$\begin{aligned} \mathrm{Left}(\Delta_t) &= i \ : \ \Delta_t^i \neq 0, \ \Delta_t^j = 0 \ \forall \ j < i \\ \mathrm{Right}(\Delta_t) &= i \ : \ \Delta_t^i \neq 0, \ \Delta_t^j = 0 \ \forall \ j > i \end{aligned} \tag{16}$$

Then the left and right edges are defined by

$$\begin{aligned} \mu_L(t) &= \frac{1}{\|\mathcal{L}\|} \sum_{s_0 \in \mathcal{L}} \mathrm{Left}(\Delta_t) \\ \mu_R(t) &= \frac{1}{\|\mathcal{L}\|} \sum_{s_0 \in \mathcal{L}} \mathrm{Right}(\Delta_t) \end{aligned} \tag{17}$$

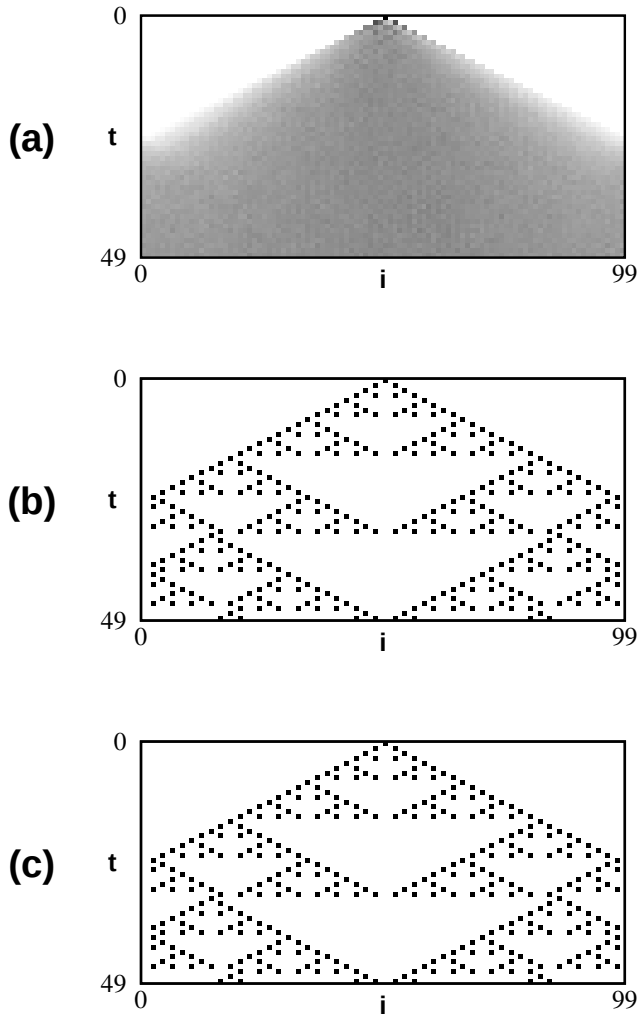

Figure 6 Difference plumes $\langle \Delta_t^i \rangle$: (a) $\mathcal{L} = \mathcal{A}^N$. Global difference plume averaged over initial conditions randomly selected over the entire state space; (b) initial conditions in domain $\mathcal{L} = \Lambda^0$; (c) initial conditions in domain $\mathcal{L} = \Lambda^1$. Note that while (a) appears to be a smooth surface, both (b) and (c) show structure. In fact, (b) and (c) are identical to the patterns of Figure 5(b) and 5(c). For each plot, $M = 1000$ pairs of states were iterated on a lattice of size $N = 100$. As above, each initial condition was perturbed in cell $j = 50$.

The Lyapunov exponents λ_L and λ_R are the linearized growth rates of $\mu_L(t)$ and $\mu_R(t)$ with time:

$$\begin{aligned} \mu_L(t) &= j + \lambda_L t + \mathcal{O}\left(t^2\right) \\ \mu_R(t) &= j + \lambda_R t + \mathcal{O}\left(t^2\right) \end{aligned} \tag{18}$$

For both of the domains, λ_L and λ_R are evidently -2 and $+2$, respectively. We measured the values for $\mathcal{A}^*$ using an ensemble of $M = 1000$ pairs of states on a lattice of size $N = 1000$. For each pair, the left- and right-most cells in which the two states differed was recorded, and the average positions $\mu_L(t)$ and $\mu_R(t)$ over the ensemble were measured. We plotted both of these quantities versus time, and fit each curve to a polynomial, identifying λ_L and λ_R with the linear terms. The values are shown in Table 1.

The third quantity associated with the difference plume is its total volume $\zeta_{\mathcal{L}}(t)$, defined as the average number of cells in which the perturbed and unperturbed states differ at time t:

$$\zeta_{\mathcal{L}}(t) = \sum_i \left\langle \Delta_t^i \right\rangle \tag{19}$$

Note that at $t = 0$, $\zeta_{\mathcal{L}}(0) = 1$ for all $\mathcal{L}$. From Figure 6(a) it is clear that $\zeta_{\mathcal{A}^*}(t)$ increases smoothly with t, while $\zeta_{\Lambda^0}(t)$ and $\zeta_{\Lambda^1}(t)$ fluctuate in an orderly but discontinuous fashion. To further illustrate this point, we show in Figure 7 a plot of $\zeta_{\mathcal{L}}(t)$ versus t for $\mathcal{L} = \Lambda^0$ and $\mathcal{L} = \mathcal{A}^*$. As expected, the curve of $\zeta_{\mathcal{A}^*}(t)$ versus t (the dashed line) increases smoothly from $\zeta_{\mathcal{A}^*}(0) = 1$, with a very slight upward curvature. A least-squares fit to a power law form $\zeta_{\mathcal{A}^*}(t) = c_1 t^{\alpha} + c_2$ gives an exponent of $\alpha = 1.03$; alternatively, fitting $\zeta_{\mathcal{A}^*}(t)$ to a polynomial gives a linear slope of $m = 1.42$. The plot of $\zeta_{\Lambda^0}(t)$ versus t, printed as a solid line, is quite different. All values of $\zeta_{\Lambda^0}(t)$ are powers of 2. Applying the above-mentioned equivalence of the difference pattern $\mathbf{\Delta}_t^{\Lambda^0}$ and the evolution of a state with a single nonzero cell under elementary CA 90, we find the exact formula

$$\zeta_{\Lambda^0}(t) = 2^{\kappa(t)} \tag{20}$$

where $\kappa(n)$ is the number of 1's in the binary expansion of n.[22] Since the difference plumes for Λ^0 and Λ^1 are identical, so are the plume volumes: $\zeta_{\Lambda^1}(t) = \zeta_{\Lambda^0}(t)$ for all t.

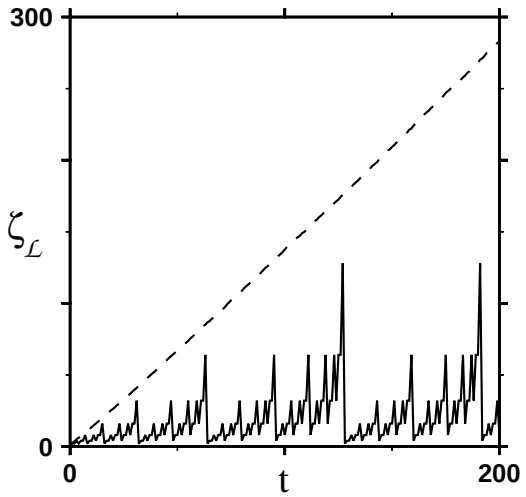

Figure 7 Difference plume volumes $\zeta_{\mathcal{L}}(t)$ versus t for the entire state space $\mathcal{L} = \mathcal{A}^*$ (dashed line) and for domain $\mathcal{L} = \Lambda^0$ (solid line). The plume volume for the other domain, $\mathcal{L} = \Lambda^1$, is identical to $\zeta_{\Lambda^0}(t)$.

4 Domain Interfaces

Having identified the regular domains Λ^0 and Λ^1 and measured their properties, it is natural to turn next to the study of the interface between two adjacent domains. This section gives a brief survey of the temporal evolution of states consisting of two domains laid side-by-side, focusing in particular on the region where they meet. We make no attempt at a complete characterization, but merely indicate the starting point. Our purpose is to illustrate the utility of analyzing the state space in terms of the pattern bases: i.e., to show how knowledge of the domains gives a new systematic view of the variety of the space-time structures—walls, dislocations, and (possibly) "particles"—that a spatial system can generate. The analysis that we indicate here has been carried out in detail for a simpler system in Ref. [11].

We are concerned with the behavior of states initially consisting of two concatenated domains Λ^i and Λ^j, with the wall between the two at a given cell m. Each domain has a specific phase,

but is otherwise chosen at random. As in Ref. [8], we denote ensembles of such "two-domain" states by $\Lambda^{i,j}$. We then allow the state to evolve, and analyze the structure of the interface between the domains. On a finite lattice, the periodic boundary conditions create another wall at cell 0, but in our investigations we will be using sufficiently large lattices that this second wall can be ignored.

One important factor in the evolution of two-domain states is the *relative phase* between the domains. This is defined as follows. Let the wall between the domains Λ^i and Λ^j be situated at cell m. Recalling the definition of the phase $\phi^i(m)$ of Λ^i from Section 2 above, define the *relative phase* $\delta\phi^{ij}$ between Λ^i and Λ^j as the difference in phase of the two domains at the wall:

$$\delta\phi^{ij} = \phi^j(m) - \phi^i(m) \tag{21}$$

Strictly speaking, the phase of Λ^i at the wall cell m is undefined, so we take $\phi^i(m)$ to be the phase that Λ^i *would have had* if the wall had not been present. For binary cell values, this latter quantity is unambiguous; extending the definition to larger alphabets requires a slight alteration of the formulation. The range of allowed values of the relative phase depends on the number of states in the process graphs of the domains on either side. For the two domains we are studying, we have $\delta\phi^{00} \in \{-1, 0, 1\}$, $\delta\phi^{01} \in \{-1, ..., 3\}$, $\delta\phi^{01} \in \{-3, ..., 1\}$, and $\delta\phi^{11} \in \{-3, ..., 3\}$. Note also that a state in $\Lambda^{i,i}$ with $\delta\phi^{ii} = 0$ does not in fact contain a wall, since the two parts of the state have the same domain type and same phase at the junction. However, for states in $\Lambda^{i,j}$ with $i \neq j$, there is a wall for all values of $\delta\phi^{ij}$. Note also that some values of relative phase are equivalent; for example, in our case, $\delta\phi^{00} = +1$ and $\delta\phi^{00} = -1$ describe the same situation. Similar degeneracies for the other domain pairs reduce the number of distinct interface types to eight, six of which are discussed below.

4.1 Interface Plots

Filtered space-time plots of six randomly selected two-domain states, representing a subset of the possible combinations of domains and relative phases, are shown in Figure 8. Examples of all four possible domain pairs $\Lambda^{i,j}$ are shown, and in addition we show two examples each of $\Lambda^{1,0}$ and $\Lambda^{1,1}$ with different values of $\delta\phi$, to investigate the importance of the relative phase. Reading the Figure from left to right, top to bottom, they are (a) $\Lambda^{0,0}$ with relative phase $\delta\phi^{00} = 1$, (b) $\Lambda^{0,1}$ with $\delta\phi^{01} = 0$, (c) $\Lambda^{1,0}$ with $\delta\phi^{10} = 0$ (d) $\Lambda^{1,0}$ with $\delta\phi^{10} = 1$, (e) $\Lambda^{1,1}$ with $\delta\phi^{11} = 1$, and (f) $\Lambda^{1,1}$ with $\delta\phi^{11} = -1$. The two interface types not shown are (g) $\Lambda^{0,1}$ with $\delta\phi^{01} = 1$ and (h) $\Lambda^{1,1}$ with $\delta\phi^{11} = 2$, for which the evolution of walls is like interfaces (a) and (e), respectively. Cells in Λ^0 are shown in white, cells in Λ^1 are gray, and all walls are black. The lattice size is $N = 1000$, of which only the central portion is displayed. Each state starts out at $t = 0$ with a single wall at cell $m = 500$.

Perhaps the most obvious feature of the plots in Figure 8 is that behavior of the interface can vary widely depending on the domains to either side. In the roughest approximation, there are two qualitatively different types of evolution: (i) spreading interface, and (ii) localized drift.

In Figures 8(a), 8(b) and 8(e), the number of walls is plainly not conserved. The single wall at $t = 0$ splits into a whole population of walls that move about, annihilate each other, and themselves split into multiple offspring. The interfacial region, i.e., the region in which walls are

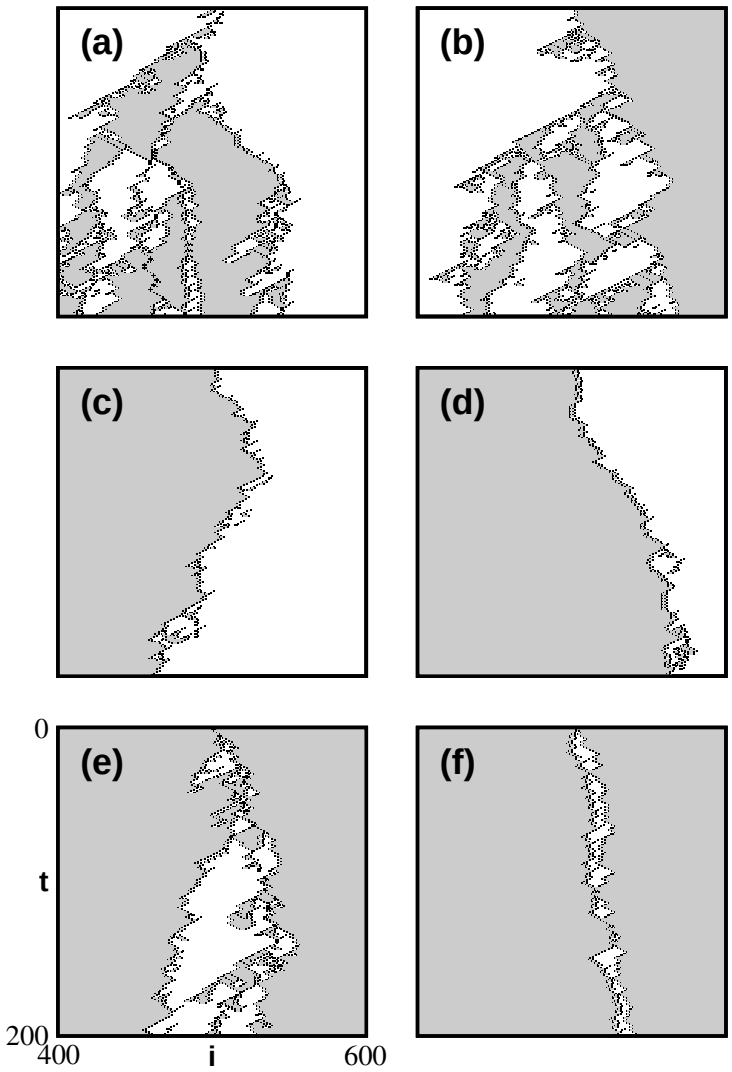

Figure 8 Evolution of domain interfaces. Each state starts out with a single wall at cell $j = 500$. The initial conditions were chosen randomly from the following ensembles: (a) $\Lambda^{0,0}$ with relative phase $\delta\phi^{00} = 1$; (b) $\Lambda^{0,1}$ with $\delta\phi^{01} = 0$; (c) $\Lambda^{1,0}$ with $\delta\phi^{10} = 0$; (d) $\Lambda^{1,0}$ with $\delta\phi^{10} = 1$; (e) $\Lambda^{1,1}$ with $\delta\phi^{11} = 1$; and (f) $\Lambda^{1,1}$ with $\delta\phi^{11} = -1$. Cells in the interior of Λ^0 are shown in white, cells in Λ^1 are gray, and all walls are black.

present, spreads rapidly to either side. In these plots, the identification of walls as "particles" is problematic at best, since the interfaces do not possess even the most basic attribute of particles, spatial localization.

In Figures 8(c), 8(d), and 8(f), on the other hand, the interfacial region remains localized in space, and drifts as a whole in one direction or another. The number of walls fluctuates but does not blow up as in the other plots. From time to time, a single wall does split into multiple offspring, but these offspring are quickly annihilated. These interfaces behave as localized "real" particles surrounded by a cloud of interacting "virtual" particles.

The diffusive character of wall motion is also immediately apparent. The walls in each plot appear to following some type of random walk, with or without a net drift. This statement will be made more quantitative in the next section.

The dependence on relative phase is illustrated in Figures 8(e) and (f). Both plots start with a state in $\Lambda^{1,1}$, but the relative phase differs. In Figure 8(e), the interface spreads, whereas in Figure 8(f), it remains localized.

4.2 Interface Plumes

The plots in Figure 8 show only a single state in each of their respective ensembles. It is possible, however, that these plots show behavior that is atypical of the ensembles. To characterize the ensembles as a whole, it is necessary to gather statistics over all the states, or at least a Monte Carlo sample of them. We do this by plotting the *interface plumes*, that is, the sum of the interfaces of the states in each two-domain ensemble. For each of the ensembles plotted in Figure 8, we generated a Monte Carlo sample of $M = 1000$ states of size $N = 1000$, and evolved each state up to time $t = 200$. The structure of the plumes is made clearer by plotting a few simple statistics, defined below. These are all measures of the positions of the walls in the interface, and are closely related to the difference plume statistics defined in the last section.

Let θ_t^i be the sign function of the output of the domain filter T_Λ upon reading the symbol σ_t^i. That is, let $\theta_t^i = 1$ whenever σ_t^i is a wall, and $\theta_t^i = 0$ otherwise. The ensemble average of θ_t^i gives the fraction of states in the ensemble $\mathcal{L}$ for which there is a wall at cell (i, t):

$$\langle \theta_t^i \rangle = \frac{1}{\|\mathcal{L}\|} \sum_{\mathrm{s}_0 \in \mathcal{L}} \theta_t^i \tag{22}$$

The roughest measure of interface evolution is just its *mean position* (or center) μ_C, defined as the average position of the walls in all states in the ensemble. This is given by the formula

$$\mu_C(t) = \sum_{i=a}^{b} i \langle \theta_t^i \rangle \tag{23}$$

with a and b chosen outside the interfacial region. The mean position will capture the average drift of the walls, but it is insensitive to the width of the interface. For this reason, we also look at the edges of the plume. For any iterate s_t of a two-domain initial condition $\mathrm{s}_0 \in \Lambda^{i,j}$ there will be a left-most and right-most wall cell. Denote these by $\mathrm{Left}(\theta_t)$ and $\mathrm{Right}(\theta_t)$, respectively. The *mean left edge* μ_L of the interface is given by the ensemble average

$$\mu_L(t) = \frac{1}{\|\mathcal{L}\|} \sum_{\mathrm{s}_0 \in \mathcal{L}} \mathrm{Left}(\theta_t) \tag{24}$$

where $\mathcal{L} = \Lambda^{i,j}$ with the chosen relative phase. Similarly, the *mean right edge* μ_R of the interface is given by

$$\mu_R(t) = \frac{1}{\|\mathcal{L}\|} \sum_{\mathrm{s}_0 \in \mathcal{L}} \mathrm{Right}(\theta_t) \tag{25}$$

The time-evolution of μ_L and μ_R measures the spreading of the interface to the left and right, respectively. The left and right spreading rates are clearly analogous to the Lyapunov exponents defined in the last section. The difference $\mu_R - \mu_L$ is a rough measure of the average interface

width. If the interface remains localized, then $\mathrm{Left}(\theta_t) \approx \mathrm{Right}(\theta_t)$ for each state in $\mathcal{L}$, and $\mu_L \approx \mu_R$.

The three quantities μ_L, μ_C and μ_R are plotted versus time in Figure 9, for the same ensembles as in Figure 8. They are the three solid lines in each plot, with $\mu_L(t) \leq \mu_C(t) \leq \mu_R(t)$ at each time t. Each plot was generated numerically using a Monte Carlo sample of the appropriate ensemble with $M = 1 \times 10^4$ states on a periodic lattice of size $N = 1000$. In addition to the mean quantities, the absolute left-most and right-most wall detected at each time are plotted as dashed lines.

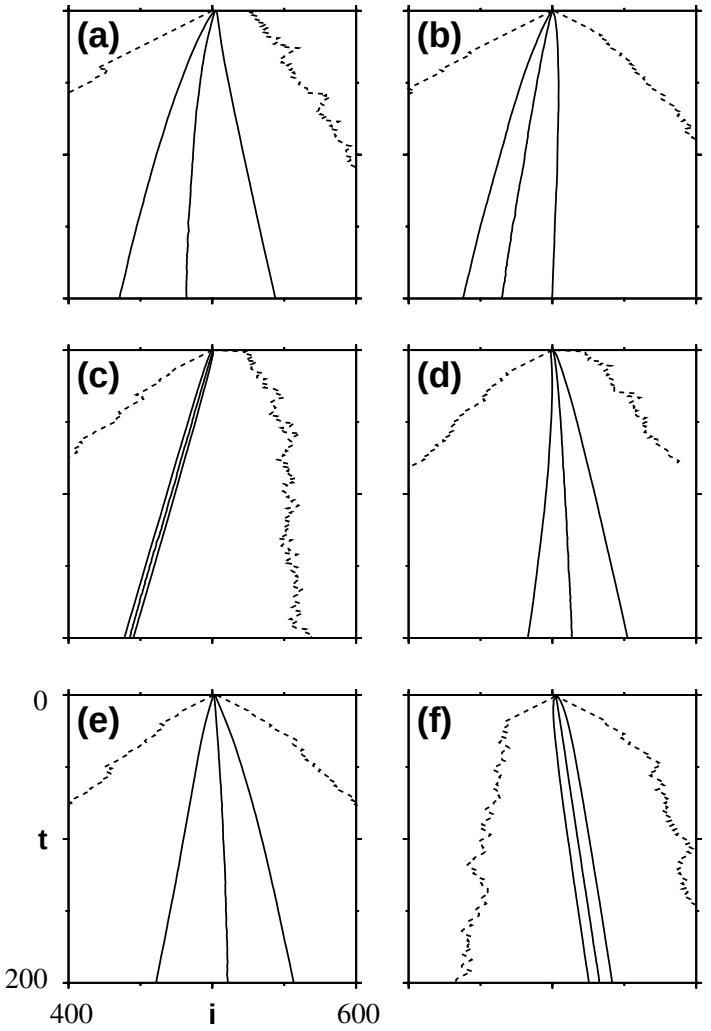

Figure 9 Interface plumes for ensembles of the six types of state shown in Figure 8. The labels (a) — (f) denote the same ensembles as in that Figure.

Figures 9(a) and 9(e) are similar, though plume (a) drifts slowly left, while plume (e) drifts slowly right. States in both of these ensembles are of the "spreading interface" type. The plume in Figure 9(b) also spreads, though more slowly than plumes (a) and (e); in addition it shows a faster net drift to the left.